JACS
JOURNAL OF THE AMERICAN CHEMICAL SOCIETY
Article
pubs.acs.org/JACS

Low-Temperature, Bottom-Up Synthesis of Graphene via a Radical-Coupling Reaction

Lang Jiang,[†,#] Tianchao Niu,[‡,#] Xiuqiang Lu,[†] Huanli Dong,[†] Wei Chen,*[,‡,§] Yunqi Liu,[†] Wenping Hu,*[,†] and Daoben Zhu[†]

[†]Beijing National Laboratory for Molecular Sciences, Key Laboratory of Organic Solids, Institute of Chemistry, Chinese Academy of Sciences, Beijing 100190, China

[‡]Department of Chemistry and [§]Department of Physics, National University of Singapore, 3 Science Drive 3, 117543, Singapore

Ⓢ *Supporting Information*

ABSTRACT: In this article, we demonstrated a method to synthesize graphene films at low temperature via a mild radical-coupling reaction. During the deposition process, with the effectively breaking of the C−Br bonds of hexabromobenzene (HBB) precursors, the generated HBB radicals couple efficiently to form graphene films at the low temperature of 220−250 °C. In situ low-temperature scanning tunneling microscopy was used to provide atomic scale investigation of the graphene growth mechanism using HBB as precursor. The chemical structure evolution during the graphene growth process was further corroborated by in situ X-ray photoelectron spectroscopy measurements. The charge carrier mobility of the graphene film grown at low temperature is at 1000−4200 $cm^2 V^{-1} s^{-1}$, as evaluated in a field-effect transistor device configuration on SiO_2 substrates, indicating the high quality of the films.

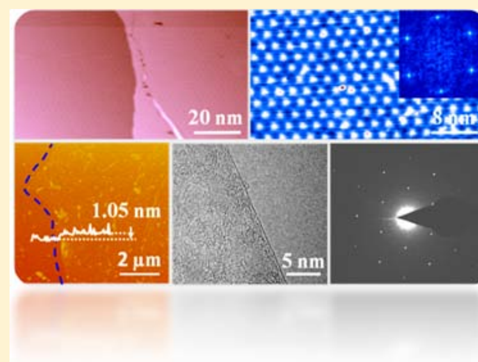

1. INTRODUCTION

Graphene is a promising candidate for next generation carbon electronics.[1] A stringent requirement to realize graphene electronics is to grow structurally perfect graphene sheets in a large area.[2−4] Different approaches have been developed to synthesize graphene and graphene nanostructures, such as the pioneer works of direct chemical synthesis,[5−9]chemical vapor deposition (CVD) of hydrocarbons on metal substrates,[10,11] epitaxial growth on single crystal metals,[12] thermal decomposition of SiC,[13] exfoliation from bulk graphite,[14] and the tailoring of graphene sheets or carbon nanotubes into nanoribbons.[15−17] The chemical bottom-up ways have attracted attention owing to the feasibility of producing large area graphene films from polymers and small molecules. However, there remains some challenges to bottom-up synthesize graphene films facilely, e.g., to synthesize graphene at low temperature. In this article, we demonstrated a bottom-up way, i.e., via a mild radical-coupling reaction, to synthesize graphene films at low temperature (220−250 °C) in a two-temperature-zone furnace.

2. EXPERIMENTAL SECTION

The low-temperature scanning tunneling microscopy (LT-STM) experiments were performed in a custom-built multichamber ultrahigh vacuum (UHV) system.[18] The Cu(111) single crystal (MaTeck, Germany) was cleaned by standard Ar^+ sputtering and annealing cycles. The surface structure and cleanliness of Cu(111) were characterized by LT-STM before the deposition of HBB molecule. Sublimation purified HBB molecules (Aldrich, 98^+%) were thermally (80 °C) evaporated from Knudsen cells (MBE Komponenten, Germany) onto the Cu(111) kept at room temperature or different elevated temperatures, monitored by a thermal couple attached. The STM imaging was carried out in constant current mode with a chemically etched W tip at 77 K. The in situ X-ray photoelectron spectroscopy (XPS) measurements were carried out in a custom-built multichamber UHV-XPS system with VSM 125 hemispherical electron analyzer.[19] The copper foils used in chemical vapor deposition (CVD) were successively cleaned with pure water, hot acetone, piranha solution (H_2SO_4/H_2O_2 = 7:3), pure water, pure isopropanol, and finally dried with high-purity nitrogen gas. The graphene samples were characterized by Raman spectroscopy (Renishaw invia plus, with laser excitation of 514 nm LabRAM HR800, with laser excitation at 514 nm), XPS (ESCALab 220I-XL), transmission electron microscopy (Tecnai G2 F20 U-TWIN).

3. RESULTS AND DISCUSSION

At the heart of graphene synthesis is how to couple benzene radicals into graphene networks (Figure 1a). Hexabromobenzene (HBB), a cheap industrial chemical, is used as the source material. When HBB solution was heated at 120 °C for 60 min (classic Ullmann coupling-reaction conditions), it quickly changed from dark-red to black (Figure 1b). The black materials are identified as carbon derivatives (Figure S1) by XPS due to the dissociation of HBB C−Br bonds even under the mild conditions.[20] In the Raman spectrum of the black products, the pronounced peaks at 1339 and 1589 cm^{-1}

Received: March 30, 2013
Published: May 23, 2013

 © 2013 American Chemical Society

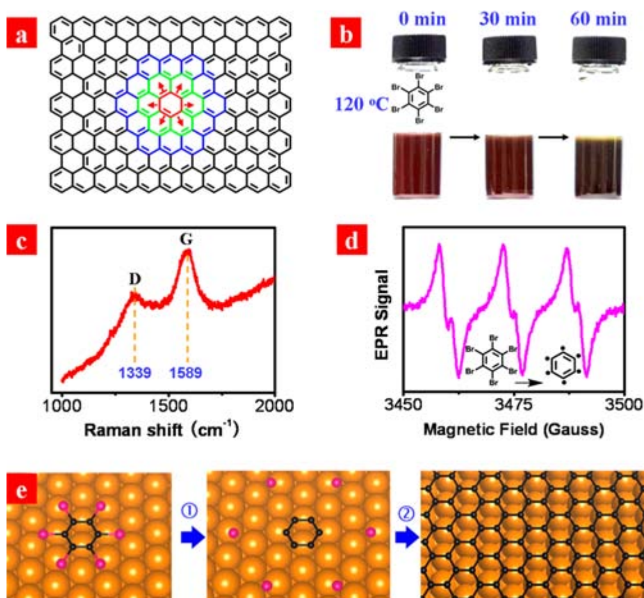

Figure 1. The synthesis of graphene from HBB with a radical cross-coupling reaction. (a) Ideal graphene structure. (b) Color changes in the HBB solution during the Ullmann radical-coupling reaction at 120 °C for 60 min. (c) Raman spectrum of the products of the HBB radical-coupling reaction. (d) EPR spectrum of aryl free radicals. (e) Schematic representation of the synthesis of monolayer graphene via the HBB radical-coupling reaction.

correspond to the D and G peaks of graphene (Figure 1c). This demonstrates the formation of nanocrystalline graphene flakes at low temperature,[21] i.e., HBB under goes a debromination reaction as the C−Br bonds[22−25] are ruptured and the resulting radicals undergo successive radical coupling to synthesize graphene derivatives. To verify the radical-coupling process, *n*-tert-butyl-α-phenylnitrone (PBN) was used as a radical trap during the Ullmann reaction. The electron paramagnetic resonance (EPR) spectrum (Figure 1d, and experimental details see Supporting Information) reveals that stable high-spin free radicals exist in the solution, i.e., the efficient generation of HBB radicals facilitate the synthesis of graphene via the radical cross-coupling reaction (Figure 1e).

In-situ LT-STM was used to monitor the HBB radical-coupling assisted growth of graphene on Cu. The room temperature deposition of HBB molecules on Cu (111) under UHV conditions immediately leads to the debromination of HBB. As shown in Figure 2a, bromine adatoms aggregate in hexagonal closely packed islands with unit cell dimensions of $a = b = 0.44$ nm, $\alpha = 60°$. These aggregated Br islands are distributed along Cu step edges and terraces[26] (see yellow rectangle in Figure 2a and the corresponding enlarged STM image in Figure 2b). This suggests that HBB undergoes the Ullmann reaction catalyzed by Cu (111). This is in good agreement with the Ullmann coupling of C_6H_5Br on Cu (111) surface at room temperature.[27]

However, due to the occupation of the active substrate surface by bromine adatoms, the decomposed carbon radicals aggregate into disordered clusters at room temperature as shown in Figure 2c. Indeed, under UHV conditions without H_2 carrier gas, high-quality graphene thin films can be grown by depositing HBB on Cu (111) at 570 °C (Figure 2d−g, at other temperature see Figure S2). The rotation of the graphene lattice with respect to the underlying Cu (111) lattice[28] results

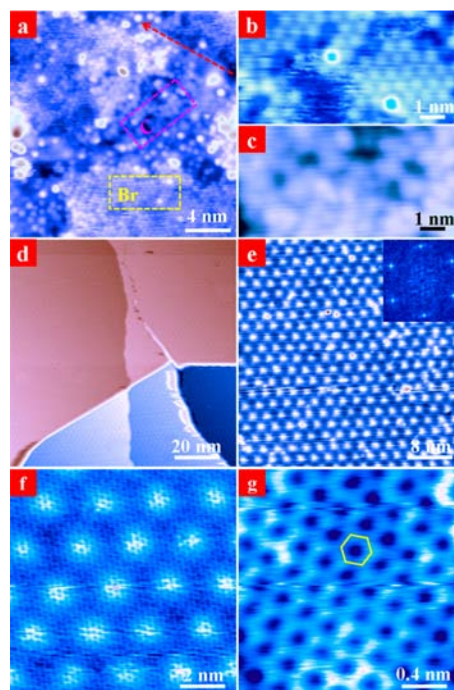

Figure 2. STM topographies of HBB radical-coupling reactions on Cu (111). (a) Initial formation of HBB clusters and bromine islands at room temperature. Pink rectangle: disordered clusters of HBB radicals; yellow rectangle: hexagonal-packed bromine-adatom islands; and red arrow indicates the step edge in the Cu substrate. (b) Magnified image of the bromine-adatom islands with hexagonal packing. (c) Magnified image of the disordered aggregated carbon clusters. (d−f) Radical-coupling assisted formation of monolayer graphene by decomposing HBB on the annealed Cu (111) at 570 °C. (d) Large-area scan of monolayer graphene on Cu (111). (e) STM image of graphene islands on Cu (111). Inset: Fourier transforms of the hexagonal super-structure. (f) Atomic resolution STM image showing periodic spacings of 2.3 nm in the Moiré pattern. (g) Atomic resolution STM image of the bright spot in (F) with honeycomb structure. Tunneling parameters: (a) V_{tip} = 0.5 V, I = 80 pA; (b) V_{tip} = 0.2 V, I = 80 pA; (c) V_{tip}=0.5 V, I = 80 pA; (d) V_{tip} = 1.2 V, I = 90 pA; (e) V_{tip} = 1.2 V, I = 80 pA; (f) V_{tip} = 1 V, I = 80 pA; (g) V_{tip} = 0.2 V, I = 90 pA.

in the appearance of a long-range ordered Moiré pattern with periodic spacing of 2.3 nm (Figure 2d−f).[29−32] The monolayer graphene honeycomb lattice can be clearly seen in Figure 2g, confirming the growth of high-quality graphene on Cu via the radical-coupling reaction at low temperature.

In situ XPS measurements were used to monitor the chemical structure evolution of the molecules involved in the decomposition processes of HBB at different temperatures. A multilayer HBB film at room temperature was used as a reference. As shown in Figure 3a, the C 1s peak of the multilayer HBB film is centered at 285.5 ± 0.05 eV with its shakeup peak at ∼290.4 ± 0.05 eV. Room temperature deposition of the monolayer HBB film on Cu foil leads to a significant broadening of the C 1s peak as compared to that of the multilayer film. The C 1s peak is centered at 284.1 ± 0.05 eV with a high-binding energy shoulder located at around of 285.5 eV.

In conjunction with our in situ STM results, the C 1s peak at 284.1 ± 0.05 eV results from the decomposition of HBB monolayer on Cu foil involving the breaking of the C−Br bond and the subsequent formation of C−C bond among the neighboring HBB radicals (Figure 2a). However, the C 1s

dx.doi.org/10.1021/ja4031825 | J. Am. Chem. Soc. 2013, 135, 9050−9054

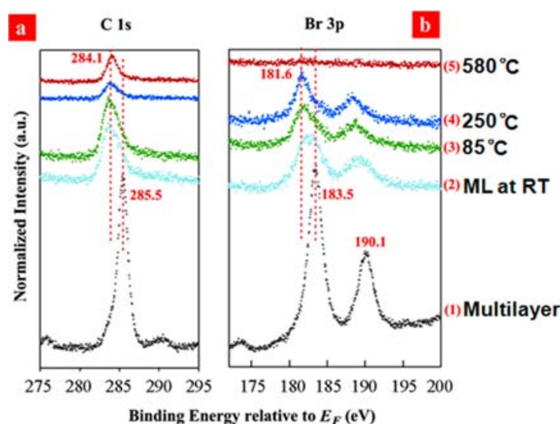

Figure 3. Core-level XPS spectra showing the evolution of HBB films on Cu foil after annealing at different temperatures: (a) C 1s and (b) Br 3p. (1) Reference multilayer HBB film grown at room temperature (RT) on Cu foil. (2) Monolayer (ML) deposit at RT. (3) ML annealed at 85 °C. (4) ML annealed at 250 °C. (5) ML annealed at 580 °C. All spectra are measured using Al Kα. All binding energy are relative to the Fermi level position of analyzer sputter-cleaned Au foil.

shoulder at higher binding energy suggests that not all HBB C−Br bonds are broken at room temperature. Further annealing of this monolayer HBB film at higher temperature leads to the gradual disapparence of the C−Br related components. After annealing at 580 °C, the C 1s spectra have a sharp peak centered at 284.1 ± 0.05 eV without a high-binding shoulder, revealing the complete decomposition of HBB molecules.

This can be further corroborated by the evolution of the Br 3p peaks. As shown in Figure 3b, when compared with that of the multilayer HBB film on Cu foil with Br 3p3/2 centered at 183.5 ± 0.05 eV, the Br 3p3/2 peak of the monolayer HBB film is much broader and extends toward lower binding energies at 181.6 ± 0.05 eV. Upon C−Br bond breaking, the Br atoms aggregate into small islands and interact strongly with the bare Cu substrate. As the Cu−Br bond possesses ionic character, the Br is more negatively charged compared with the Br in the C−Br bond, and hence the Br 3p3/2 shifts toward lower binding energies. Upon annealing the HBB monolayer to 250 °C, the C−Br component almost vanishes, indicating that all C−Br bonds at this temperature are broken. With further annealing to 580 °C, we could not detect any visible Br components, suggesting that Br atoms evaporate from Cu substrates upon high-temperature annealing. Our in situ STM and XPS results reveal that graphene formation using HBB as a precursor competes with the adsorption of released Br from HBB on Cu, i.e., the formation of high-quality graphene films requires the complete desorption of Br on Cu which allows a free Cu surface to catalyze the HBB radicals into graphene. This suggests that it is necessary to design a proper synthesis process to avoid or prevent the adsorption of released Br atoms on Cu surfaces during the reaction. Fortunately, in the CVD process, the dissociated H_2 on Cu at elevated temperature can interact with Br and to promote the desorption of these decomposed Br, thereby emptying the Cu surface for the graphene growth.

Large-area graphene films were synthesized based on the radical-coupling reaction in a two-zone furnace of a physical vapor transport system (Figure S3). HBB was sublimed at low temperatures (100−150 °C), and the radicals were transported with H_2/Ar carrier gas and deposited on substrates in the high-temperature zone (220−250 °C). The sublimation of HBB was accurately controlled at 0.035 mg/min, i.e., 2.8 molecules/($nm^2 \cdot s$).

A graphene films of 3 × 3 cm^2 was transferred onto a silicon wafer with 300 nm-thick SiO_2. The thickness of this graphene layer, measured by AFM, is 1.05 nm (Figure 4a). The TEM

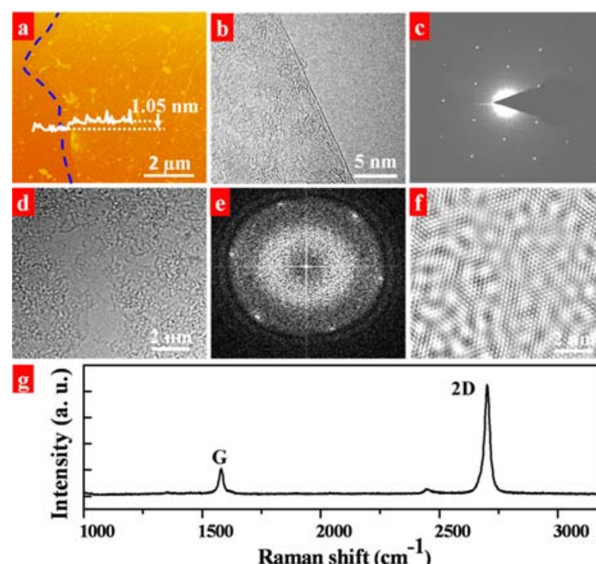

Figure 4. Graphene films synthesized by vacuum radical-coupling reaction. (a) AFM image of the d 1.05 nm-thick monolayer graphene film. (b) TEM image of the monolayer graphene film. (c) The corresponding SAED pattern of the monolayer graphene film shows a the hexagonal structure of the (0001) basal plane. (d) A 2D FFT of the film. (e) FFT image showing the diffraction pattern. The six spots indicate that the graphitic layers are aligned with the Cu lattice planes (spacing 0.21 nm). (f) The reconstructed image after filtering the noise in the frequency domain. (g) The Raman spectrum of the monolayer graphene.

image of the monolayer graphene film is shown in Figure 4b, and the corresponding selected area electron diffraction (SAED) pattern, shown in Figure 4c, illustrates the hexagonal structure of the (0001) basal plane. The same SAED pattern was obtained at different parts of the same film. A two-dimensional (2D) fast Fourier transform (FFT) was performed on this film (i.e., on the same film in the TEM image in Figure 4d). The FFT of a single hexagonal graphene network produces six spots of 0.21 nm spacing (Figure 4e). Figure 4f showed the image reconstructed by filtering in the frequency domain to remove unwanted noise. The Raman spectrum of monolayer graphene is shown in Figure 4g. The two sharp peaks in this spectrum are the G peak at 1580 cm^{-1} and the 2D peak at 2701 cm^{-1}. The I_{2D}/I_G intensity ratio is 4, and the full-width at half-maximum (fwhm) of the 2D peak is 30 cm^{-1}. The D peak (1350 cm^{-1}) is weak, suggesting the absence of sp^3 carbon atoms and defects. Raman spectral mapping (Figure S4) showed a very weak D band and very sharp and uniform G and 2D bands; the 2D band at 2700 cm^{-1} has a fwhm of 35−55 cm^{-1}, indicating the high quality of the graphene films.[33,34]

The quality of the obtained graphene films was further evaluated by the electrical transport measurements in a field-effect transistor configuration.[35−37] Bottom gate, top contact transistor devices of the graphene films were fabricated on Si/SiO_2 (300 nm) substrates (low-resistance Si as the back gate) by thermally evaporating Au films as source and drain electrodes (Figure 5). Transistor arrays based on the graphene

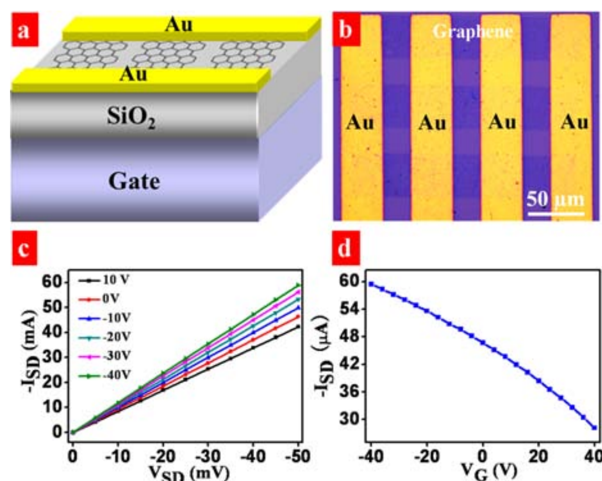

Figure 5. Schematic illustration and electrical properties of graphene transistors. (a) Schematic diagram of a field-effect transistor on Si/SiO2 (300 nm) substrates with Au as source and drain electrodes. (b) Microscopy image of transistor arrays on the graphene film. (c) Graphene transistors current output at different voltages. (d) Typical output and transfer characteristics.

film are shown in Figure 5a,b. All devices were measured at room temperature. The typical output and transfer characteristics of the devices are shown in Figure 5c,d. We have fabricated 50 devices. The measured mobilities are in the range of 1000−4200 cm^2 V^{-1} s^{-1}, which are comparable to that of previously reported CVD-grown graphene.[10,38,39] The high mobility of the transistors indicates the high quality of the graphene films.

4. CONCLUSION

In summary, we demonstrated a mild radical-coupling reaction to synthesize graphene films at low temperature (220−250 °C). With the debromination of HBB, the generated benzene radicals coupled into graphene films efficiently at low temperature. Such growth mechanism was further corroborated by in situ LT-STM and XPS investigations. The graphene films showed sharp G peak at 1580 cm^{-1} and 2D peak at 2701 cm^{-1} with I_{2D}/I_G intensity ratio of 4. Field-effect transistors based on the graphene films and Si/SiO_2 substrates exhibit hole mobility up to 4200 cm^2 V^{-1} s^{-1}.

■ ASSOCIATED CONTENT

Supporting Information

Description of the material included. This material is available free of charge via the Internet at http://pubs.acs.org.

■ AUTHOR INFORMATION

Corresponding Author

phycw@nus.edu.sg; huwp@iccas.ac.cn

Author Contributions

#These authors contributed equally.

Notes

The authors declare no competing financial interest.

■ ACKNOWLEDGMENTS

W.H. appreciated the profound discussion with Prof. Eiichi Nakamura (Tokyo University) and Dr. Xinliang Feng (Max Planck Institute for Polymer Research). The authors acknowledge the financial support from the National Natural Science Foundation of China (20721061, 51033006, 51222306, 51003107, 61201105, 91027043, 91222203, 91233205), the China-Denmark Coproject (6091130231), TRR61 (NSFC-DFG Transregio Project), the Ministry of Science and Technology of China (2011CB808400, 2011CB932300, 2013CB933403, 2013CB933500), Chinese Academy of Sciences and Singapore ARF grants R143-000-505-112, R143-000-530-112, R143-000-542-112, and NUS YIA grant R143-000-452-101.

■ REFERENCES

(1) Geim, A. K.; Novoselov, K. S. *Nat. Mater.* **2007**, *6*, 183−191.
(2) Bonaccorso, F.; Sun, Z.; Hasan, T.; Ferrari, A. C. *Nat. Photonics* **2010**, *4*, 611−622.
(3) Pan, Y.; Zhang, H.; Shi, D.; Sun, J.; Du, S.; Liu, F.; Gao, H. *Adv. Mater.* **2009**, *21*, 2777−2780.
(4) Sutter, P. *Nat. Mater.* **2009**, *8*, 171−172.
(5) Sun, Z.; Yan, Z.; Yao, J.; Beitler, E.; Zhu, Y.; Tour, J. M. *Nature* **2010**, *468*, 549−552.
(6) Cai, J.; Ruffieux, P.; Jaafar, R.; Bieri, M.; Braun, T.; Blankenburg, S.; Muoth, M.; Seitsonen, A. p.; Saleh, M.; Feng, X.; Müllen, K. *Nature* **2010**, *466*, 470−473.
(7) Chen, L.; Hernandez, Y.; Feng, X. L.; Mullen, K. *Angew. Chem., Int. Ed.* **2012**, *51*, 7640−7654.
(8) Dossel, L.; Gherghel, L.; Feng, X. L.; Mullen, K. *Angew. Chem., Int. Ed.* **2011**, *50*, 2540−2543.
(9) Englert, J. M.; Hirsch, A.; Feng, X. L.; Mullen, K. *Angew. Chem., Int. Ed.* **2011**, *50*, A17−A24.
(10) Li, X.; Cai, W.; An, J.; Kim, S.; Nah, J.; Yang, D.; Piner, R.; Velamakanni, A.; Jung, I.; Tutuc, E.; Banerjee, S.; Colombo, L.; Ruoff, R. *Science* **2009**, *324*, 1312−1314.
(11) Lin, Y. M.; Dimitrakopoulos, C.; Jenkins, K. A.; Farmer, D. B.; Chiu, H. Y.; Grill, A.; Avouris, Ph. *Science* **2010**, *327*, 662−662.
(12) Mao, J.; Huang, L.; Pan, Y.; Gao, M.; He, J.; Zhou, H.; Guo, H.; Tian, Y.; Zou, Q.; Zhang, L.; Zhang, H.; Wang, Y.; Du, S.; Zhou, X.; Neto, A. H. C.; Gao, H. *Appl. Phys. Lett.* **2012**, *100*, 093101.
(13) Emtsev, K.; Bostwick, A.; Horn, K.; Jobst, J.; Kellogg, G. L.; Ley, L.; Mcchesney, J. L.; Ohta, T.; Reshanov, S. A.; Röhr, J.; Rotenberg, E.; Schmid, A. K.; Waldmann, D.; Weber, H.; Seyller, T. *Nat. Mater.* **2009**, *8*, 203−207.
(14) Novoselov, K. S.; Geim, A. K.; Morozov, S. V.; Jiang, D.; Zhang, Y.; Dubonos, S. V.; Grigorieva, I. V.; Firsov, A. A. *Science* **2004**, *306*, 666−669.
(15) Li, X.; Wang, X.; Zhang, L.; Lee, S.; Dai, H. *Science* **2008**, *319*, 1229−1232.
(16) Jiao, L.; Zhang, L.; Wang, X.; Diankov, G.; Dai, H. *Nature* **2009**, *458*, 877−880.
(17) Wei, D.; Xie, L.; Lee, K. K.; Hu, Z.; Tan, S.; Chen, W.; Sow, C. H.; Chen, K. Q.; Liu, Y.; Wee, A. T. S. *Nat. Commun.* **2013**, *4*, 1374.
(18) Chen, W.; Li, H.; Huang, H.; Fu, Y.; Zhang, H. L.; Ma, J.; Wee, A. T. *J. Am. Chem. Soc.* **2008**, *130*, 12285−12289.
(19) Zhong, J. Q.; Huang, H.; Mao, H. Y.; Wang, R.; Zhong, S.; Chen, W. *J. Chem. Phys.* **2011**, *134*, 154706.
(20) Walch, H.; Gutzler, R.; Sirtl, T.; Eder, G.; Lackinger, M. *J. Phys. Chem. C* **2010**, *114*, 12604−12609.
(21) Ferrari, A. C.; Robertson, J. *Philos. Trans. R. Soc., A* **2004**, *362*, 2477−2512.
(22) Rapson, W. S.; Shuttleworth, R. G. *Nature* **1941**, *147*, 675.
(23) Xi, M.; Bent, B. E. *J. Am. Chem. Soc.* **1993**, *115*, 7426−7433.
(24) Grill, L.; Dyer, M.; Lafferentz, L.; Persson, M.; Peters, M. V.; Hecht, S. *Nat. Nanotechnol.* **2007**, *2*, 687−691.
(25) Krasnikov, S. A.; Doyle, C. M.; Sergeeva, N. N.; Preobrajenski, A. B.; Vinogradov, N. A.; Sergeeva, Y. N.; Zakharov, A. A.; Senge, M. O.; Cafolla, A. A. *Nano Res.* **2011**, *4*, 376−384.
(26) Nanayakkara, S. U.; Sykes, E. C. H.; Fernandez-Torres, L. C.; Blake, M. M.; Weiss, P. S. *Phys. Rev. Lett.* **2007**, *98*, 206108.

(27) Blake, M. M.; Nanayakkara, S. U.; Claridge, S. A.; Fernandez-Torres, L. C.; Sykes, C. H.; Weiss, P. S. *J. Phys. Chem. A* **2009**, *113*, 13167−13172.
(28) Gao, L.; Guest, J. R.; Guisinger, N. P. *Nano Lett.* **2010**, *10*, 3512−3516.
(29) Chen, X.; Liu, S.; Liu, L.; Liu, X.; Liu, X.; Wang, L. *Appl. Phys. Lett.* **2012**, *100*, 16310.
(30) Merino, P.; Svec, M.; Pinardi, A. L.; Otero, G.; Martin-Gago, J. A. *ACS Nano* **2011**, *5*, 5627−5634.
(31) Bao, Q.; Zhang, H.; Wang, B.; Ni, Z.; Lim, C, H. Y. X.; Wang, Y.; Tang, D. Y.; Loh, K. P. *Nat. Photonics* **2011**, *5*, 411−415.
(32) Lu, J.; Castro Neto, A. H.; Loh, K. P. *Nat. Commun.* **2012**, *3*, 823.
(33) Schwab, M. G.; Narita, A.; Hernandez, Y.; Balandina, T.; Mali, K. S.; De Feyter, S.; Feng, X. L.; Mullen, K. *J. Am. Chem. Soc.* **2012**, *134*, 18169−18172.
(34) Wang, X.; Li, X.; Zhang, L.; Yoon, Y.; Weber, P.; Wang, H.; Guo, J.; Dai, H. *Science* **2009**, *324*, 768−771.
(35) Ed. Hu, W. *Organic Optoelectronics*; Wiley-VCH: Weinheim, Germany, 2013.
(36) Wang, C.; Dong, H.; Hu, W.; Liu, Y.; Zhu, D. *Chem. Rev.* **2012**, *112*, 2208−2267.
(37) Wen, Y.; Liu, Y.; Guo, Y.; Yu, G.; Hu, W. *Chem. Rev.* **2011**, *111*, 3358−3406.
(38) Wu, B.; Geng, D.; Xu, Z.; Guo, Y.; Huang, L.; Xue, Y.; Chen, J.; Yu, G.; Liu, Y. *NPG Asia Mater.* **2013**, *5*, e36.
(39) Li, X.; Magnuson, C. W.; Venugopal, A.; Tromp, R. M.; Hannon, J. B.; Vogel, E. M.; Colombo, L.; Ruoff, R. S. *J. Am. Chem. Soc.* **2011**, *133*, 2816−2819.